Calibration and experimental verification of discrete element parameters of Panax notoginseng root

Kaiting Xie[1,2], Zhaoguo Zhang[1,2*], Fa'an Wang[2], Xiaolan Yu[2,3], Chenglin Wang[2], Shifei Jiang[1,4]

(1. *Faculty of Mechanical and Electrical Engineering, Kunming University of Science and Technology, Kunming 650500, China*;
2. *Faculty of Modern Agricultural Engineering, Kunming University of Science and Technology, Kunming 650500, China*;
3. *Guizhou Agricultural Machinery Technology Promotion Station, Guiyang 550003, China*;
4. *Yunnan Tobacco Machinery Co., Ltd, Kunming 650100, China*)

Abstract: Existing discrete element method-based simulation analysis of Panax notoginseng root soil separation still has the challenge to get the accurate and reliable basic parameters, which are necessary for discrete element simulation. In this paper, the P. notoginseng roots suitable for harvesting period were taken as the experimental object. Then using 3D scanning reverse modeling technology and EDEM software to establish the discrete element model of P. notoginseng, based on which, the physical and virtual tests were carried out to calibrate the simulation parameters. First, the basic physical parameters (density, triaxial geometric size, moisture content, shear modulus, and elastic modulus) and contact coefficients (static friction coefficient, rolling friction coefficient, and crash recovery coefficient between P. notoginseng roots and 65Mn steel) were measured by physical tests. Furthermore, treating the contact coefficients of P. notoginseng roots as the influence factor, the steepest uphill test, and four factors combing five levels of rotational virtual simulation are conducted. The measured relative error accumulation angle and simulation accumulation angle are set as the performance indices. The results show that the static friction coefficient, rolling friction coefficient, crash recovery coefficient, and surface energy coefficient of P. notoginseng roots are 0.55, 0.35, 0.16, and 19.5 J/m^2, respectively. Using calibration results as parameters of the vibration separation simulation test of P. notoginseng soil, the Box-Behnken vibration separation simulation tests were carried out, in which the vibration frequency, inclination angle, and vibration amplitude of separation device as factors, screening rate and damage rate of P. notoginseng soil complex are regarded as indices. The results show that the optimal operating parameters of the separation device are the vibration frequency of 10 Hz, the inclination angle of 5°, and the amplitude of 6 cm. Based on the optimal operation parameters, the discrete element simulation experiment and field experiment of P. notoginseng roots soil separation are also performed to compare the soil three-dimensional trajectory space coordinates of P. notoginseng roots. From the results, three axis coordinate error is less than 15%. This proves that the calibration results are reliable. It can also provide the theoretical basis and technical support for the further study of the P. notoginseng root soil separation platform.

Keywords: Panax notoginseng, root, EDEM, parameter calibration, separation test
DOI: 10.25165/j.ijabe.20241704.8122

Citation: Xie K T, Zhang Z G, Wang F, Yu X L, Wang C L, Jiang S F. Calibration and experimental verification of discrete element parameters of Panax notoginseng root. Int J Agric & Biol Eng, 2024; 17(4): 13–23.

1 Introduction

Panax notoginseng is a perennial herb of the family Araliaceae, mainly produced in Yunnan Province, China. As a traditional precious Chinese medicinal material, P. notoginseng has shown the important medicinal and health care value[1]. Traditional experimental methods cannot accurately analyze the movement process of P. notoginseng roots in harvesting machinery, which makes the P. notoginseng harvesting equipment performs worse than that of other root crops. This seriously restricts the mechanization progress of P. notoginseng industry.

In recent years, the discrete element method is widely used in the study of medium material movement process. However, the effectiveness of discrete element method's results mainly depends on the accurate material parameters[2-5]. Therefore, it is necessary to calibrate the intrinsic parameters and contact coefficients when the agricultural material model is simulated[3,6,7]. Hence, it is crucial to systematically study the P. notoginseng root discrete element parameters for the optimization design of root-soil separation equipment of the P. notoginseng harvester.

The most mature and widely used method is to obtain the optimal values of discrete element simulation parameters by measuring intrinsic parameters, physical parameters, and contact parameters of materials and carrying out accumulation angle test. For dry materials, the core of parameter calibration lies in the establishment of physical model. For spherical or near spherical materials, EDEM can be directly used to preset spherical particles as simulation models, such as wheat flour[8] and soybean[9,10].

Received date: 2023-07-14 **Accepted date:** 2023-12-29
Biographies: **Kaiting Xie**, PhD, research interest: intelligent agricultural machinery equipment, Email: xkt@stu.kust.edu.cn; **Fa'an Wang**, PhD, research interest: intelligent agricultural equipment design and manufacturing, Email: wfa@kust.edu.cn; **Xiaolan Yu**, master, research interest: intelligent agricultural machinery equipment, Email: 2577760557@qq.com; **Chenglin Wang**, PhD, research interest: intelligent agricultural machinery equipment, Email: wangchenglin055@163.com; **Shifei Jiang**, PhD, research interest: intelligent agricultural machinery equipment, Email: 20212203008@stu.kust.edu.cn.
***Corresponding author: Zhaoguo Zhang**, Professor, PhD Supervisor, research interest: intelligent agricultural equipment design and manufacturing. Faculty of Modern Agricultural Engineering, Kunming University of Science and Technology, No.727, Jingming South Road, Chenggong District 650500, China. Tel: +86-15911701001, Email: zzg@kust.edu.cn.

Domestic and foreign scholars obtain 3D models of materials with irregular shapes and small individual differences by 3D drawing software and 3D scanner, and then obtain discrete meta model by using EDEM software. Such as oil sunflower grain[11], ice grass seed[12], wheat grain[13], cotton[14], water chestnuts[15], rape offal[16], alfalfa straw[17] and wheat straw[18] and other material parameters calibration. Researchers usually establish multiple 3D models to simulate materials with irregular shapes and differences between individuals to improve the accuracy of parameter calibration. Such as peanut seeds[19], flax seeds[20], corn[21], pear[22], etc. For sticky materials, the selection of adhesion model between particles is particularly important. Hertz-Mindlin with JKR contact model is mostly used for parameter calibration of viscous soil and fertilizer, which can better simulate the adhesion between wet particles. For example, post-tillage soil in Xinjiang[23], lattice-red soil in Hainan hot area[24], pig manure organic fertilizer treated by black fly[25] and organic fertilizer applied mechanically[26], etc. The Edinburgh Elasto-Plastic Adhesion contact model is a nonlinear elastic-plastic contact model, which can simulate relatively dry particles more accurately. Such as no-till soil[27,28]. However, the common contact model of EDEM software cannot better simulate the cohesion characteristics of grapevine cold protection soil. Researchers have integrated hysteretic spring contact model (HSCM). The liner cohesion model (LCM) is used as the contact model between soil particles to improve the accuracy of parameter calibration[29].

In summary, discrete element methods have been maturely applied in the field of parameter calibration of materials with single shape. However, the shapes of P. notoginseng roots are different, and the winding of fibrous roots improves the randomness of parameter calibration values. Therefore, it is difficult to obtain the accurate parameters by only using a single model and physical test. In order to prevent the distortion of the simulation effect, in this paper, first, the discrete meta model of the P. notoginseng root was established by the 3D scanning technology and the JKR contact model. After that, the discrete element parameters are calibrated, thereby guaranteeing the optimal values for the vibration separation simulation test of P. notoginsen root and soil. Finally, the field experiment was conducted to verify the reliability of the simulation model and parameters. The research can provide a basis for the design and parameters optimization of harvesting machinery of P. notoginseng.

2 Establishment of discrete element model of P. notoginsen root

In this section, P. notoginseng physical parameters (density, moisture content, shear strength) required for the discrete element simulation test are measured, and the obtained parameters provide data support for establishing a discrete element model.

2.1 Density and moisture content

The density of P. notoginsen root was measured by drainage method[30]. The experiment was repeated, and the average density of samples measured in four sampling sites was used as the root density of P. notoginsen. The measurement results are the average density of P. notoginsen root is 1.23 g/cm^3.

The air blast drying method was used to measure the moisture content of P. notoginseng root[31]. According to the calculation, the average water content of mature P. notoginseng roots were 71.99%.

2.2 Shear modulus and elastic modulus

The shear strength is obtained through direct shear test, expressed as Equation (1) [32]:

$$p_{jp} = |c_p| + f_p \tan\varphi_p \quad (1)$$

where, p_{jp} is the shear strength of P. notoginseng root, kPa; is the cohesive force of P. notoginseng root, kPa; f_p is the positive pressure, kPa; φ_p is the angle of internal friction of P. notoginseng root, (°).

The sample was sheared by the shear device, as shown in Figure 1. The shear modulus of P. notoginseng was calculated through Figure 2 as 9.58 MPa. The vertical stress corresponding to the maximum shear strength of each root and stem was calculated, and the linear fitting of stress and shear strength resulted in Equation (2) as follows:

$$P_{jp} = 0.5296 f_p - 23.79 \quad (2)$$

According to Equations (1) and (2), the friction angle and cohesion of P. notoginseng root were 27.9° and 23.79 kPa, respectively. According to Equation (3), the average value of elastic modulus is 20.118 Mpa.

$$S = E/2(1+p) \quad (3)$$

where, S is the shear modulus, Mpa; E is the elastic modulus, MPa; p is Poisson's ratio, The Poisson ratio of P. notoginseng root is 0.05[32].

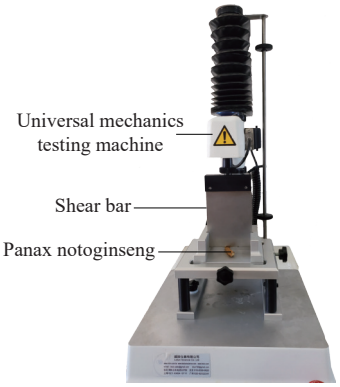

Figure 1 Test of shearing P. notoginseng

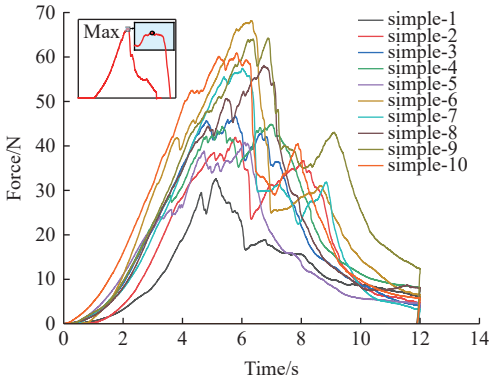

Figure 2 Shear stress-time plot

2.3 Establishment of discrete element model of P. notoginseng root based on 3D scanning

In this paper, EXScan S-Shning three-dimensional scanning was used to conduct 360° all-round scanning of the scanned object, and the data point set of the appearance of the scanned object was obtained, as shown in Figures 3a-3c. The model can simulate the root damage of P. notoginseng well, so the model was applied to the vibration separation simulation test of P. notoginseng root soil. Figure 3d shows the simplified P. notoginseng model, which only retains the main root of P. notoginseng, which can eliminate the

experimental error caused by the winding of P. notoginseng fiber root in the calibration process of contact parameters. Therefore, the model was used for calibration test of contact parameters of P. notoginseng.

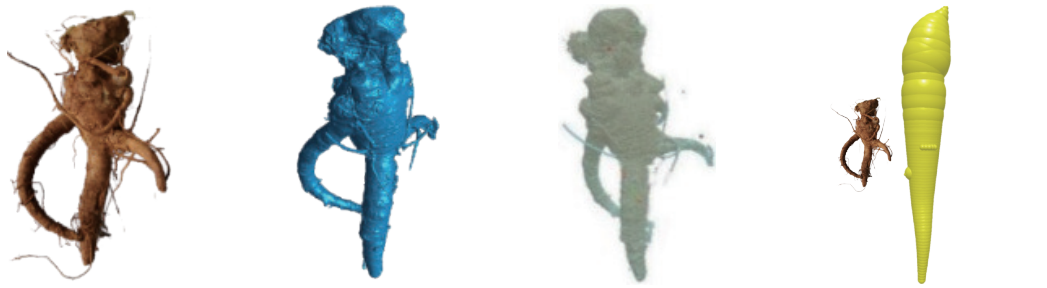

a. P. notoginseng root b. 3D model c. Discrete element model d. Simple discrete element model

Figure 3 Construction process of discrete element model of P. notoginsen root

3 Determination of contact parameters between P. notoginseng root and 65Mn

3.1 Contact material selection

The separation screen of P. notoginseng harvester adopts 65Mn material, therefore, the contact parameters between P. notoginseng root and 65Mn were determined. The simulation parameters of 65Mn[23] and soil[33] are listed in Table 1.

Table 1 Discrete element simulation model parameters

Parameter	65Mn steel	Soil
Poisson's ratio	0.35	0.4
Shear modulus/Pa	7.27×10^{10}	1.61×10^{10}
Density/(kg·m^{-3})	7830	1332

3.2 Static friction coefficient

The static friction coefficient between two objects is measured by the inclined plane test. As shown in Figure 4a, the root of P. notoginseng was placed on the horizontal 65Mn plate, and the plane tilt angle was slowly changed. The Qian Yanlang high-speed photography equipment was used to record the movement process of P. notoginseng, and the included angle of the plane when P. notoginseng started to slide on 65Mn was measured. The parameters were extracted by high-speed video target tracking measurement software V1.0, according to Equation (4)[24]. Calculate the static friction coefficient. After 20 repeated experiments, the average sliding friction angle between P. notoginseng root and 65Mn was 11.5°, and the static friction coefficient was 0.203.

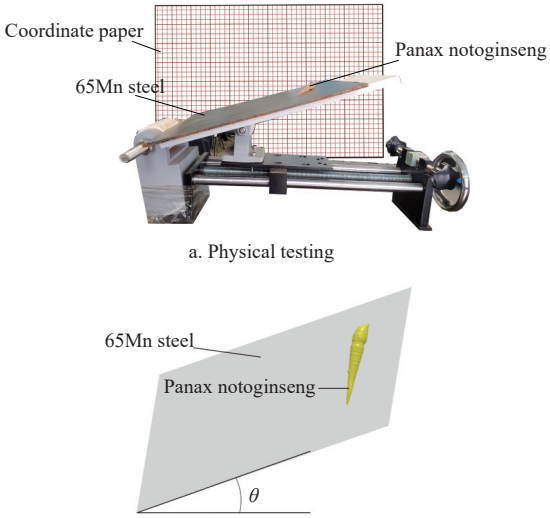

a. Physical testing

b. Simulated test

Figure 4 Calibration test of static friction coefficient between P. notoginseng and 65Mn

$$\left.\begin{aligned} F_1 &= G\sin\theta \\ F_2 &= G\cos\theta \\ F_1 - f &= 0 \\ F_2 - N &= 0 \\ f &= \mu F_2 \end{aligned}\right\} \tag{4}$$

where, F_1 is the opposite force of frictional force between P. notoginseng and the plane, N; F_2 is the pressure of P. notoginseng on the plane, N; G is the gravitational force of P. notoginseng, N; f is the frictional force between P. notoginseng and the plane, N; N is the support force of the plane on the P. notoginseng, N; μ is the coefficient of static friction between P. notoginseng-contact material; θ is the critical angle of rolling friction, (°).

In the EDEM test showed as Figure 4b, the contact coefficients except the static friction were set to 0, the exact slip angle θ was taken as the test index, and the static friction element was taken as the test coefficient. The static friction coefficient ranged from 0.1 to 0.5, with an interval of 0.05. Nine groups of simulation tests were conducted, and each group was repeated 10 times, and the mean value was taken. The static friction coefficient μ and the critical slip angle θ were fitted (Figure 5).

The fitting equation is

$$\mu = 0.005 + 0.016\theta + 8.64\times10^{-5}\theta^2 (R^2 = 0.999\,71) \tag{5}$$

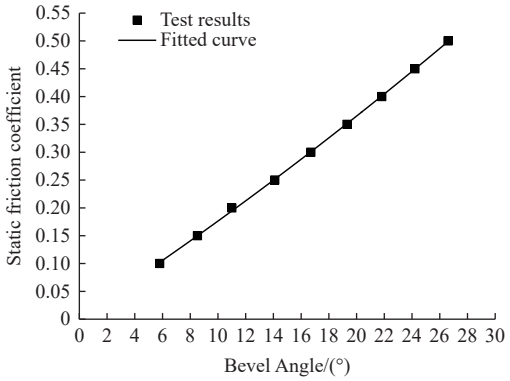

Figure 5 Fitting curves of staic friction coefficient and inclination angle

When the measured sliding friction angle was 11.5° in Equation (5), the static friction coefficient was 0.199, and the error was small. Therefore, the static friction coefficient between P. notoginseng root and 65Mn was defined as 0.199.

3.3 Coefficient of rolling friction

The coefficient affecting the sliding distance of P. notoginseng is called the rolling friction coefficient, which can be calculated by Equation (6)[34].

$$Gl\sin\theta_1 = G(l\cos\theta_1 + L)\rho \tag{6}$$

where, G is the mass of P. notoginseng, g; l is the distance from the initial point to the bottom of the inclined plane, i.e. the rolling distance of P. notoginseng on the inclined plane, mm; θ_1 is the inclination angle of the plate, (°); L is the distance of P. notoginseng root sliding on the plane, mm; ρ is the rolling friction coefficient.

After several pre-experiments, the angle of the plane was adjusted and fixed to 50°, and the rolling distance L of the inclined plane was 30 mm. This guarantees the radix P. notoginseng root could roll from the plane without jumping (Figure 6a). The horizontal rolling distance of 20 groups of P. notoginseng root was measured and the average value was calculated. The average slip distance is 2.52 mm, and the rolling friction coefficient between P. notoginseng root and 65Mn is 1.053.

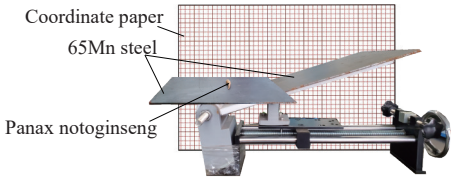

a. Physical testing

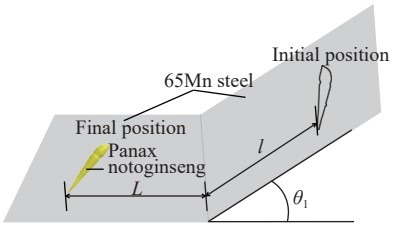

b. Simulated test

Figure 6 Calibration test of rolling friction coefficient between P. notoginseng and 65Mn

The contact coefficients except the rolling friction and static friction in the EDEM test (Figure 6b), is set to 0, and the static friction is set to 0.2. The plane sliding distance l is selected as the test index, and the rolling friction coefficient is selected as the test variable for the validation test. The range of the rolling friction coefficient is 0.75-1.15, and the interval is selected as 0.05. Nine groups of simulation test are conducted. Each group of simulation is repeated 10 times, and take the average. The static friction coefficient ρ was fitted to the critical slip angle θ_1 (Figure 7).

The fitting equation is

$$\rho = 1.19 - 0.05L + 0.001L^2 (R^2 = 0.999\,87) \tag{7}$$

When the measured slip distance of P. notoginseng root 2.52 mm was substituted into Equation (7), the rolling friction coefficient was calculated as 1.07, and the simulated test error was small. Therefore, the rolling friction coefficient between P. notoginseng and 65Mn was defined as 1.07.

3.4 Coefficient of crash recovery

As shown in Figure 8, P. notoginseng bounces back after colliding with materials. According to the formula defined by the coefficient of restoration, it can be simplified into Equation (8)[34].

$$e = \frac{v_1}{v_2} = \frac{\sqrt{2gh}}{\sqrt{2gH}} = \frac{\sqrt{h}}{\sqrt{H}} \tag{8}$$

where e is the crash recovery factor; v_1 is the rebound normal velocity, mm/s; g is the acceleration of gravity, 9.8 m/s^2; v_2 is the fall normal velocity, mm/s; h is the maximum rebound height, mm; H is the fall height, taken as 400 mm.

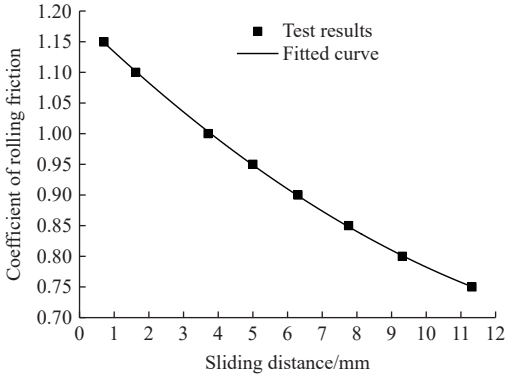

Figure 7 Fitting curve of rolling friction coefficient and slip distance

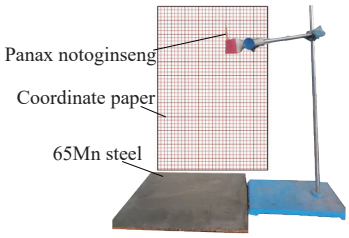

a. Physical testing

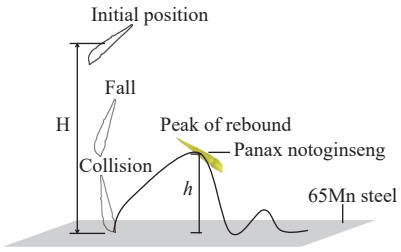

b. Simulated test

Figure 8 Calibration test of crash recovery coefficient between *P. notoginseng* and 65Mn

The highest rebound height of P. notoginseng root was recorded by the high-speed photography. The ratio between the height and the falling height was the crash recovery coefficient P. notoginseng root and 65Mn (Figure 8a). After repeated experiments for 20 times, the average value of the highest rebound height between P. notoginseng root and 65Mn was 13 mm, and the calculated crash recovery coefficient was 0.18.

The static friction coefficient and rolling friction coefficient between P. notoginseng root and 65Mn were set as 0.2 and 1.07, respectively. Taking the crash recovery coefficient as the test variable, and the highest rebound height of the root and stem of P. notoginseng was selected as the test index. The crash recovery coefficient was set as 0.14-0.22 with an interval of 0.01. Nine groups of simulation tests were conducted. The simulation process is shown in Figure 8b. The crash recovery coefficient and the highest rebound height were fitted in Figure 9.

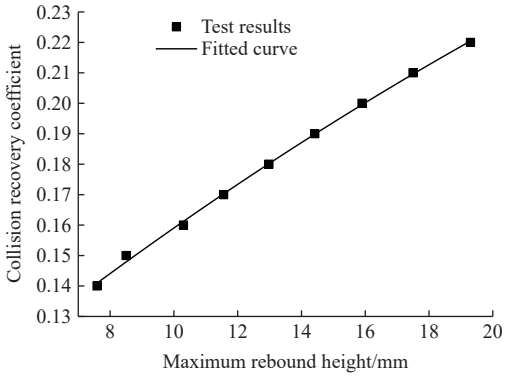

Figure 9 Fitting curve of recovery coefficient and maximum springing height

The fitting equation is

$$e = 0.078 + 0.0086h - 7.73 \times 10^{-5} h^2 (R^2 = 0.998\ 74) \quad (9)$$

By substituting the measured maximum rebound height of 13 mm into Equation (9), the crash recovery coefficient is 0.177, and the simulated test error is small. Therefore, the crash recovery coefficient between P. notoginseng and 65Mn is defined as 0.177.

4 Calibration of contact parameters between roots of P. notoginseng

4.1 Real stacking angle test

According to the standard of "Determination of Accumulation angle of Bulk Material"[35], the accumulation angle of P. notoginseng was measured by funnel method[36]. The test samples were taken from Honghe Maitreya. After repeated measurement for 10 times (Figure 10), the average accumulation angle of panax notoginseng root was 36.1°, and the specific data are listed in Table 2.

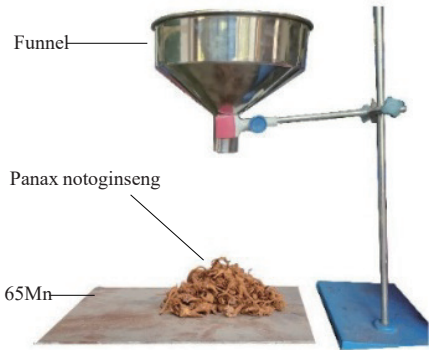

Figure 10 Stacking angle test

Table 2 Stacking angle measurement data

IDX	Angle/(°)	IDX	Angle/(°)
1	35.6	6	36.0
2	37.1	7	36.4
3	36.3	8	35.1
4	36.1	9	36.2
5	35.9	10	36.4

4.2 Steepest climb test

The funnel was drawn using Solidworks and the funnel parameters were set to be consistent with the actual one to carry out the simulated stacking angle test. This is shown in Figure 11. Before numerical simulation, the acquired physical parameters (density, moisture content, etc.) were fixed. And the remaining parameter ranges of P. notoginseng were retrieved from the GEMM material parameter database. X is the P. notoginseng-P. notoginseng crash recovery coefficient, ranging from 0.14 to 0.18; Y is the P. notoginseng-P. notoginseng static friction coefficient, ranging from 0.4 to 0.6; Z is the P. notoginseng-P. notoginseng dynamic friction coefficient, ranging from 0.2 to 0.5; J is the P. notoginseng-P. notoginseng surface energy, ranging from 16 to 20 J/m^2. Using the relative error of the measured stacking angle of P. notoginseng rootstock as the test index, the steepest climb test was designed as listed in Table 3. The maximum and minimum values of each parameter are set as the boundary in the tests. The same interval value was taken within the parameter range and conducting the test in turn. Compare the test results with the performance index to find the test group with the smallest error. Then the parameters near the test group with the smallest error were chosen as the test parameters to conduct the orthogonal test according to the test needs. In this study, the optimal group of parameters and another four groups of parameters in its vicinity were selected to carry out orthogonal tests.

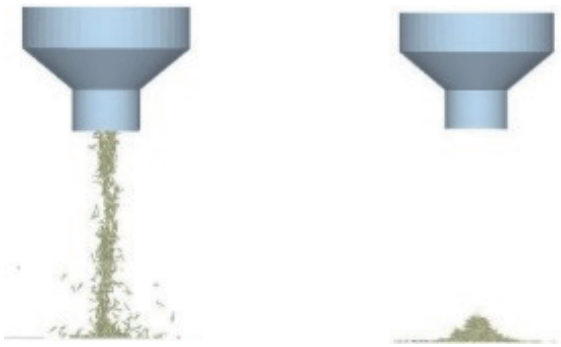

Figure 11 Stacking angle simulation test

Table 3 Design and results of steepest climb test scheme

IDX	Factors				Evaluation index	
	X	Y	Z	J/(J·m^{-2})	Stacking angle/(°)	Relative error/%
1	0.140	0.400	0.200	16.0	21.26	41.1
2	0.145	0.425	0.2375	16.5	24.18	33.0
3	0.150	0.450	0.275	17.0	20.34	43.7
4	0.155	0.475	0.3125	17.5	22.32	38.2
5	0.160	0.500	0.350	18.0	28.16	22.0
6	0.165	0.525	0.3875	18.5	39.43	9.20
7	0.170	0.550	0.425	19.0	31.44	13.0
8	0.175	0.575	0.4625	19.5	31.30	13.3
9	0.180	0.600	0.500	20.0	32.20	10.8

Note: X in the table is the P. notoginseng-P. notoginseng crash recovery coefficient, Y is the P. notoginseng-P. notoginseng static friction coefficient, Z is the P. notoginseng-P. notoginseng dynamic friction coefficient and J is the P. notoginseng-soil surface energy.

4.3 Orthogonal test

The analysis of Table 3 showed that the relative error measured in the 6 th group was the smallest. And the 4th, 5th, 7th and 8th groups near the 6 th group were taken as the optimal interval to design a four-factor, five-level orthogonal test. The factor-level coding table is listed in Table 4.

Table 4 Horizontal coding table of orthogonal test factors

Level	Factors			
	X	Y	Z	J/(J·m^{-2})
1	0.155	0.475	0.3125	17.5
2	0.160	0.500	0.3500	18.0
3	0.165	0.525	0.3875	18.5
4	0.170	0.550	0.4250	19.0
5	0.175	0.575	0.4625	19.5

In Table 5, R characterizes the influence level of the test factors on the test index. The larger the value of R is, the greater the influence is. The value of K indicates the relative error under different combinations of the factors. The smaller the value of K is, the smaller the relative error is. As can be seen from Table 5, the effects of the four factors on the stacking angle of P. notoginseng were X, J, Y and Z in descending order. The parameters corresponding to the smallest values of k_1, k_2, k_3, k_4 and k_5 were taken as the optimal levels of the P. notoginseng-P. notoginseng contact coefficients. The P. notoginseng-P. notoginseng crash recovery coefficient, P. notoginseng-P. notoginseng static friction coefficient, P. notoginseng-P. notoginseng dynamic friction coefficient and P. notoginseng-P. notoginseng surface energy were 0.16, 0.55, 0.35 and 19.5 J/m^2. Using these parameters, the EDEM P. notoginseng pellet accumulation angle test was carried out again, resulting in an accumulation angle of 35.8°, with a relative error of 0.8% from the measured value.

Table 5 Design and results of orthogonal experiment

IDX	Factors				Evaluation index
	X	Y	Z	J/(J·m^{-2})	Relative error/%
1	1	1	1	1	41.1
2	1	2	2	2	33.0
3	1	3	3	3	43.7
4	1	4	4	4	38.2
5	1	5	5	5	22.0
6	2	1	2	3	9.2
7	2	2	3	4	33.0
8	2	3	4	5	13.3
9	2	4	5	1	10.8
10	2	5	1	2	33.0
11	3	1	3	5	41.1
12	3	2	4	1	33.0
13	3	3	5	2	21.0
14	3	4	1	3	38.2
15	3	5	2	4	42.0
16	4	1	4	2	33.0
17	4	2	5	3	29.0
18	4	3	1	4	32.0
19	4	4	2	5	21.0
20	4	5	3	1	13.0
21	5	1	5	4	45.0
22	5	2	1	5	19.0
23	5	3	2	1	20.0
24	5	4	3	2	16.0
25	5	5	4	3	31.0
Relative error/%	k_1 1.780	1.694	1.633	1.179	
	k_2 0.993	1.470	1.252	1.360	
	k_3 1.753	1.300	1.468	1.511	
	k_4 1.280	1.242	1.485	1.902	
	k_5 1.310	1.410	1.278	1.164	
	R 0.787	0.452	0.381	0.738	

5 Validation tests

5.1 EDEM vibrational separation test on P. notoginseng root-soil complex

5.1.1 Parameter setting and model construction

To verify the feasibility of calibrated parameters. EDEM P. notoginseng root-soil complex vibration separation test was further carried out. The calibrated parameters were assigned to the P. notoginseng root-soil discrete element model, and the P. notoginseng planting soil discrete element parameters are listed in Table 6. A simplified three-dimensional model of the separation sieve was drawn using Solidworks and imported into EDEM software. The separation sieve material intrinsic parameters were set to 65Mn, and the contact coefficients with P. notoginseng were the calibrated parameters.

Table 6 Soil contact parameter

Serial number	Name of parameter	Numerical value
1	Coefficient of static friction	0.98
2	Dynamic friction factor	0.16
3	JKR surface energy	14.52J·m^{-2}
4	Recovery coefficient	0.73

The JKR model was chosen to describe the interactive dynamics between P. notoginseng and soil, and soil to soil. The default spherical particle model in EDEM was used to simulate soil particles in the experiment. Based on the measured soil particle sizes and distribution ratios The proportions of single spherical particles, double spherical particles and triple spherical particles were set according to the measured soil particle sizes and distribution ratios, as listed in Table 7[37].

Table 7 Basic shape parameters of soil discrete element model

Ratio	33.1%	24.9%	42%
Particle shape			

In this section, a complete discrete element model of P. notoginseng was encapsulated and filled, and the physical and contact parameters of the soil particles are set, then produce a root-soil complex, as shown in Figure 12.

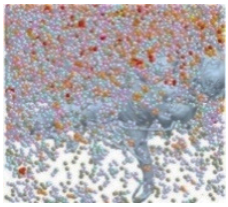

a. Root-soil composite filling process

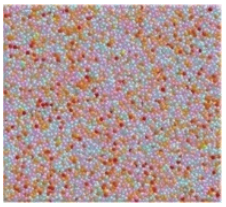

b. Root-soil composite filled

Figure 12 Formation process of P. notoginseng soil complex

5.1.2 Test procedure and analysis of results

The simulation time was set to 3 s with a step size of 0.01 s. When analysing the rate of wounded P. notoginseng, the number of intact P. notoginseng particles in calculation domains Ⅰ and Ⅱ is recorded as undamaged P. notoginseng particles. And the number of damaged P. notoginseng particles consists of the P. notoginseng particles separated by vibration in calculation domains 2 and the particles already dropped in calculation domain Ⅲ. The sum of all particles in the calculation domain is the number of intact P. notoginseng particles (Figure 13).

Similarly, change the counted particles to soil particles and leave the rest of the settings unchanged. The soil particles in calculation domains Ⅰ and Ⅱ in Figure 14 that are not adhered to the P. notoginseng root, plus the soil particles in calculation domain Ⅲ that have been sieved off, will be recorded as the total number of sieved soil particles. The number of particles in all calculation domains is the total number of soil particles.

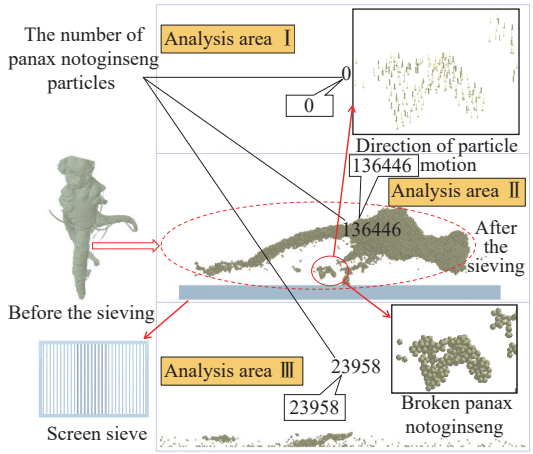

Figure 13 Particle number of P. notoginseng before and after vibration separation

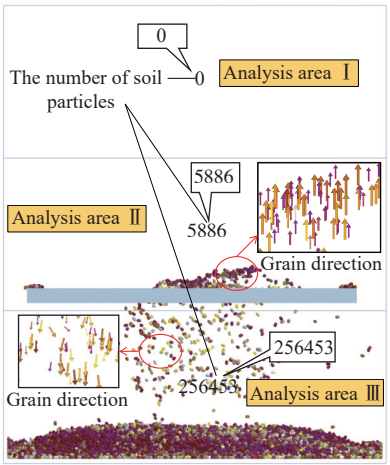

Figure 14 Number of soil particles before and after vibration separation

The net sieve rate is calculated from Equation (10). It accorded to Equation (11) to obtain the wounded P. notoginseng rate.

$$\phi = (N_s - n_s)/N_s \tag{10}$$

$$\psi = (N_p - n_p)/N_p \tag{11}$$

where, φ is the net sieving rate,%; ψ is the percentage of injured P. notoginseng,%; N_s is the number of soil particles before sieving; n_s is the number of soil particles after sieving; N_p is the number of P. notoginseng particles before sieving; n_p is the number of P. notoginseng particles after sieving.

Taking the vibration frequency, inclination angle, and the vibration amplitude of the separation device as the test variables, and the damage rate and screening rate of P. notoginseng as the test indices, the Box-Behnken test was designed. The simulation test factors and levels are listed in Table 8.

Table 8 Box-Behnken test factor coding

Level	Vibration separation test factors		
	A-Vibrational frequency/Hz	B-Inclination of separation device/(°)	C-Vibration amplitude/cm
–1	5	0	5
0	7.5	2.5	7.5
1	10	5	10

The Box-Behnken vibration separation process is listed in Table 9, and the Box-Behnken vibration separation test scheme and test results are listed in Table 10. When t=0.5 s, the separation device just started to vibrate, the P. notoginseng root-soil complex was subjected to vibration. The BONDING bond between the soil particles would break under the external force, and the soil particles fell off from the P. notoginseng root stem. At t=1 s, with the increase of vibration time, the damage of soil and P. notoginseng rootstock became more obvious. At t=1.5 s, the bond between P. notoginseng and soil also failed due to vibration, and the buried P. notoginseng rootstock particles were exposed. This achieves the effect of root-soil separation. At t=2 s, a large number of soil particles adhering to P. notoginseng roots broke away from the surface of the roots. The adhering soil was then reduced, and the P. notoginseng roots were also broken due to the vibration. After 2.5 s, the vibration was stopped, and the soil particles suspended in the air were left to fall freely. The simulation was turned off at 3 s.

Table 9 Vibration separation process

IDX	Time/s	Separation of soil complexes from P. notoginseng root	Damage to the P. notoginseng root
1	0.5		
2	1		
3	1.5		
4	2		
5	2.5		
6	3		

Table 10 Box-Behnken test scheme and results

IDX	Factors			Evaluation index	
	A/Hz	B/(°)	C/cm	ϕ/%	ψ/%
1	5.0	0	7.5	54.20	0.90
2	10.0	0	7.5	93.20	3.86
3	5.0	5.0	7.5	50.10	1.05
4	10.0	5.0	7.5	90.20	4.30
5	5.0	2.5	5.0	38.70	0.40
6	10.0	2.5	5.0	90.13	3.36
7	5.0	2.5	10.0	58.30	1.38
8	10.0	2.5	10.0	95.40	4.43
9	7.5	0	5.0	70.92	2.63
10	7.5	5.0	5.0	66.90	2.63
11	7.5	0	10.0	82.40	3.66
12	7.5	5.0	10.0	72.00	4.07
13	7.5	2.5	7.5	80.30	3.12
14	7.5	2.5	7.5	79.41	2.98
15	7.5	2.5	7.5	74.50	3.12
16	7.5	2.5	7.5	73.20	3.12
17	7.5	2.5	7.5	80.01	3.14

Note: A is the vibration frequency of the separation device, Hz; B is the inclination angle of the vibrating screen, (°); C is the vibration amplitude of the vibrating screen, cm; ϕ is the net sieving rate of P. notoginseng root and soil complex,%; ψ is the injury rate of P. notoginseng,%.

A multiple regression was fitted to the test data using Design-Expert 8.0.6 software, and the regression equation for the net screening rate of the vibrating separation unit was obtained as

Equation (12).

$$\phi = 0.79 + 0.21a - 0.022b + 0.056c - 0.000\,341\,2ab - 0.031ac - 0.02bc - 0.0510a^2 - 0.015b^2 - 0.026c^2 \quad (12)$$

The regression equation for the injury rate for the vibration separation method is Eq.(13):

$$\psi = 2.01 + 1.03a + 0.086b + 0.38c + 0.026ab + 0.022ac + 0.063bc - 0.48a^2 + 0.12b^2 + 0.01c^2 \quad (13)$$

The significance test of the regression variance is listed in Table 11. Table 11 shows that the vibration frequency of the separation device and the vibration amplitude of the separation device have a significant effect on the net sieve rate and the injury rate of P. notoginseng. The tilt angle of the separation device has a greater effect on the injury rate than on the net sieve rate. The fitted model for the sieve net rate is $R^2 = 0.9885$, and the predicted values of the regression equation fitted well with the actual values. Three factors that had a decreasing effect on the net sieve rate were: vibration frequency, vibration amplitude and inclination of the separation device. The fitted model $R^2 = 0.9981$ for the injury rate of P. notoginseng presented a good fitting result. The three factors that had a decreasing effect on the net rate of root soil screening were vibration frequency, vibration amplitude and inclination of the separation device. The two-by-two interaction response surfaces are shown in Figures 15 and 16.

Table 11 Variance analysis of circular separation screen

Soruces of variation	Sieve net rate				Injury rate of P. notoginseng root			
	Quadratic sum	DOF	ϕ	ψ	Quadratic sum	DOF	ϕ	ψ
Model	0.39	9	66.90	< 0.0001**	10.82	9	408.88	< 0.0001**
a	0.34	1	524.68	< 0.0001**	8.56	1	2911.40	< 0.0001**
b	0.004	1	5.84	0.0463*	0.060	1	20.23	0.0028**
c	0.025	1	38.41	0.0004**	1.18	1	402.00	< 0.0001**
ab	4.66E-07	1	0.0007	0.9793	0.003	1	0.93	0.3668
ac	0.004	1	5.99	0.0442*	0.002	1	0.66	0.4445
bc	0.002	1	2.55	0.1544	0.02	1	5.36	0.0538*
a^2	0.011	1	16.72	0.0046**	0.96	1	326.43	< 0.0001**
b^2	0.001	1	1.55	0.2527	0.06	1	20.38	0.0028**
c^2	0.003	1	4.42	0.0735*	0.0004	1	0.15	0.7105
Residual	0.003	7			0.02	7		
Lack of fit	0.002	3	0.77	0.5697	0.02	3	4.21	0.0993
Error	0.003	4			0.005	4		
Sum	0.39	16			10.84	16		

Note: The symbol * stands for significant and ** stands for extremely significant.

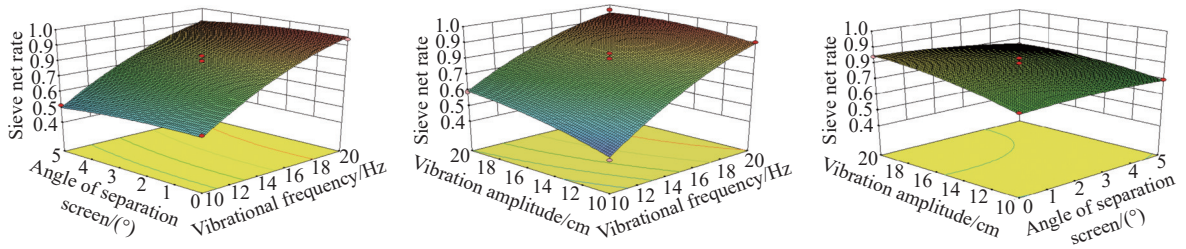

a. Inclination of separation device-vibration frequency b. Vibration amplitude-vibration frequency c. Vibration amplitude-inclination of separation device

Figure 15 Response surface of screening rate for vibration separation

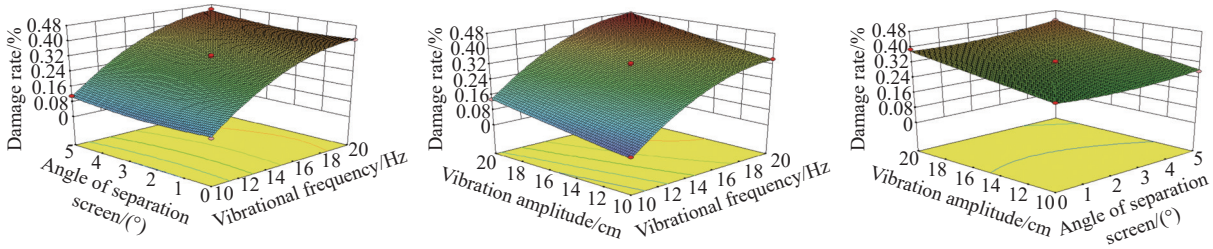

a. Inclination of separation device-vibration frequency b. Vibration amplitude-vibration frequency c. Vibration amplitude-inclination of separation device

Figure 16 Vibration separation damage rate response surface of P. notoginseng

The optimum combination of parameters was calculate by the Optimization-Numerical module of the Design-Expert 8.0.6 software and optimization condition (14).

$$\left.\begin{aligned}\phi &= (38.7, 95.44)_{\max}\\ \psi &= (0.4, 4.43)_{\min}\end{aligned}\right\} \quad (14)$$

The optimum operating parameters of the vibratory separation device were the vibration frequency of 10 Hz, the tilt angle of the separation device of 5°, and the vibration amplitude of 6 cm. At this point, the predicted sieving rate was 90.1% and the injury rate was 2.22%. The results will be used to verify the accuracy of the P. notoginseng root and soil parameters set in the simulation tests.

5.2 Field trials and analysis

5.2.1 Test equipment and prep

In order to assess the accuracy of simulation parameters, a number of experiments were conducted in field. This section describes the details of these experiments, obtained results for all the methods and discussion on these results.

The trial site was located in Shilin Yi Autonomous County, Kunming City, Yunnan Province, with a latitude of 24°55′4″, a longitude of 103°19′44″ and an altitude of 1933 m. The agronomic characteristics of P. notoginseng cultivation, with low shade shelters and stakes inserted between the monopolies, prevented direct harvesting. Hence, some of the shade shelters and stakes were removed, as shown in Figure 17. As the root-soil complex model did not include P. notoginseng stems in the simulation test, the P. notoginseng stems in the test area were removed to reduce interference, thereby ensuring the accuracy of the test data. Then the movement of the P. notoginseng root-soil complex can be captured more clearly, as shown in Figure 18.

Figure 17 P. notoginseng plantation after the removal of shade

Figure 18 Artificial seedling killing treatment

5.2.2 Test procedure

A suspended 4U-2 P. notoginseng harvester with a rated engine power of 36.8 kW and an overall mass of 300 kg was used for harvesting, with an operating efficiency of 0.1 hm^2/h. As shown in Figure 19, the driver was seated in the tractor cockpit in front of the harvester to manipulate the speed, lift angle, vibration frequency, and amplitude of the harvester. P. notoginseng roots laid on the ground after excavation.

a. In the digging b. After digging

Figure 19 Operation process of traction *P. notoginseng* harvester

High-speed photography was used to record the movement of P. notoginseng on the bar, as shown in Figure 20. The P. notoginseng was moved up and down due to the vibration of the bar. At the same time, the soil on the P. notoginseng root was partially separated, but not completely separated. Using the high-speed photographic post-processing software, the root-soil complex of P. notoginseng was selected, its motion coordinates were derived and the 3D trajectory was plotted.

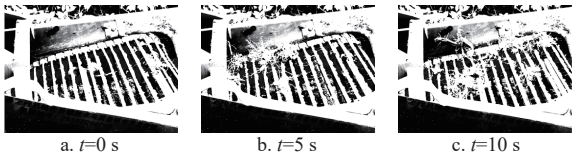

a. t=0 s b. t=5 s c. t=10 s

Figure 20 The motion process of P. notoginseng on the separation device was photographed at high speed

5.2.3 Analysis of test results

(1) Verification of P. notoginseng roots movement patterns based on high-speed photography

Because the reference coordinate system of crop movement in the field experiment is not consistent with that in the simulation experiment, a comparison of the spatial trajectory range was used in order to verify the accuracy of the simulation results. We only required the observation of the range of X, Y and Z axis coordinate values in the simulation and the test in 3D coordinates. To visually compare the difference between the two trajectory ranges, the actual P. notoginseng motion trajectory was panned without deformation to reduce the space occupied by the two trajectories when they share the same 3D coordinate axis. This could make the simulated trajectory consistent with the actual trajectory as much as possible. Then the three-axis motion boundary values were compared, which is more intuitive and does not affect the data results. The 3D diagram of the trajectory after translation is shown in Figure 21.

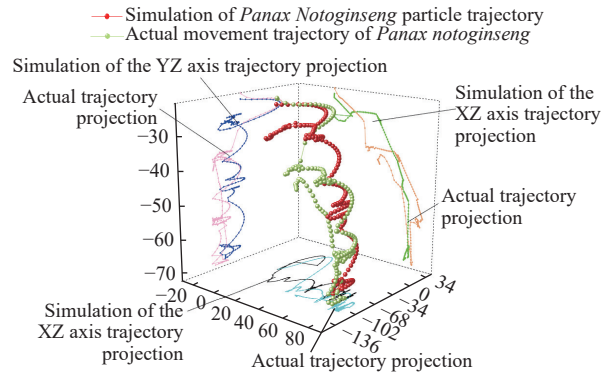

Figure 21 Simulation of actual comparison of movement track of P. notoginseng

Analysis of Table 12 shows that the errors of X, Y and Z coordinates between the simulated and actual P. notoginseng are 11.54%, 12.24%, and 5.35% respectively. The error of trajectory is less than 15%. The simulated situation is consistent with the actual situation. And the error of P. notoginseng motion range in the Z-axis direction is the smallest, which is less than 10%. This indicates that the motion characteristics of P. notoginseng along the force direction are basically the same under the same direction of action and force.

Table 12 Simulation - Actual motion range of P. notoginseng

Coordiate axis	Coordinate values of P. notoginseng particles are simulated/mm			The actual coordinate value of P. notoginseng/mm		
	Max	Min	Dif	Max	Min	Dif
X	71.34	2.90	68.45	81.08	3.71	77.38
Y	13.30	–96.88	110.17	15.72	–109.81	125.54
Z	–22.6	–70.38	47.79	–20.81	–71.29	50.49

(2) Verification of soil movement patterns based on high-speed photography

A three-dimensional view of the soil trajectory is shown in Figure 22. Analysis of Table 13 shows that the movement errors of the soil particles in *X*, *Y*, and *Z* directions between the simulation and the actual field trial were 4.87%, 2.33% and 3.95% respectively, which are less than 5%. The simulated soil parameters are accurate.

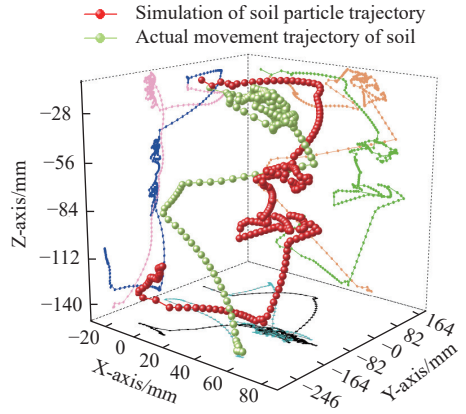

Figure 22 Simulation of actual soil movement trajectory

Table 13 Simulation - Actual soil motion range

Coordiate axis	Simulated soil particle coordinate values/mm			Actual soil particle coordinates/mm		
	MAX	MIN	DIF	MAX	MIN	DIF
X	–14.37	–69.6	55.23	–17.88	–70.55	52.67
Y	101.12	–260	360.58	110.24	–242.12	352.36
Z	–16.94	–147	129.97	–11.58	–146.89	135.31

6 Conclusions

1) The physical characteristic parameters of P. notoginseng were measured by experiments. The average density of P. notoginseng was 1.23 g/cm^3. The average diameter and moisture content are 24.59 mm and 71.99%, respectively. The friction angle, cohesion and elastic modulus are 27.9°, 23.79 kPa and 20.118 MPa, respectively.

2) Contact parameters coefficients (static friction coefficient, rolling friction coefficient, and crash recovery recovery coefficient between P. notoginseng roots and 65Mn steel) were measured by physical and virtual tests as 0.199, 1.07 and 0.177, respectively. Furthermore, P. notoginseng roots were tested at an accumulation angle of 36.1°. The steepest climb test and four-factor combing five-level orthogonal test were carried out to obtain the optimal parameters, in which the stacking angle of 36.1° is set as the test index. P. notoginseng-P. notoginseng crash recovery coefficient, static and dynamic friction coefficients, and surface energy are 0.16, 0.55, 0.35 and 19.5 J/m^2 respectively. It can provide a basis for setting contact parameters between P. notoginseng and 65Mn.

3) The discrete element model of P. notoginseng-soil-separation device was established using EDEM, and the Box-Behnken vibration separation test was carried out. The optimal operating parameters of the vibration separation device were vibration frequency of 10 Hz, inclination angle of the separation device of 5° and vibration amplitude of 6 cm.

4) A field P. notoginseng harvesting test was carried out to extract the trajectories of P. notoginseng and soil, which are compared with the simulation results. It was found that the error range of soil and P. notoginseng trajectories in the simulation test was less than 15%, which proved that the parameters calibrated in this paper were accurate and reliable. P. notoginseng discrete element parameters calibrated in this study can be directly applied to P. notoginseng harvest, root-soil separation, and other discrete element simulation tests, and the accurate P. notoginseng model provides a guarantee for the design optimization test of P. notoginseng digging device and root-soil separation device.

Acknowledgements

The authors acknowledge that this research was financially supported by National Key R&D Program of China (Grant No. 2022YFD2002004), Yunnan Fundamental Research Projects (Grant No. 202401CF070144), and “Xingdian Talent Support Program” Youth Talent Project of Yunnan Province (Grant No. KKXX202423055).

[References]

[1] Li J B, Bao Y L, Wang Z, Yang Q, Cui X M. Research progress in diseases of Panax notoginseng. Physiological and Molecular Plant Pathology, 2022; 121: 101878.

[2] Coetzee C J. Review calibration of the discrete element method. Power Technology, 2017; 310: 104–142.

[3] Fu J, Chen Z, Han L J, Ren L Q. Review of grain threshing theory and technology. Int J Agric & Biol Eng, 2018; 11(3): 12–20.

[4] Turkia S B, Wilke D N, Pizette P, Govender N, Abriak N E. Benefts of virtual calibration for discrete element parameter. Granular Matter, 2019; 21(110): 1–16.

[5] Yang Q Z, Shi L, Shi A P, He M S, Zhao X Q, Zhang L, Addy M. Determination of key soil characteristic parameters using angle of repose and direct shear stress test. Int J Agric & Biol Eng, 2023; 16(3): 143-150.

[6] Zhang Z G, Zeng C, Xing Z Y, Xu P, Guo Q F, Shi R M, Wang Y Z. Discrete element modeling and parameter calibration of safflower biomechanical properties. Int J Agric & Biol Eng, 2024; 17(2): 37–46.

[7] Yu Y, Diao L S, Wang D W, Wang J S, Wang X M, Tan X Z, Yi D Z. Lightweight design of peanut sowing machine frame based on finite element analysis. Int J Agric & Biol Eng, 2023; 16(3): 120–129.

[8] Li Y X, Li F X, Xu X M, Shen C P, Meng K P, Chang D T. Parameter calibration of wheat flour for discrete element method simulation based on particle scaling. Transactions of the CSAE, 2019; 35(16): 320–327. (in Chinese)

[9] Khatchatourian O A, Binelo M O, de Lima R F. Simulation of soya beanflow in mixed-flow dryersusing DEM. Biosystems Engineering, 2014; 123: 68–76.

[10] Peng C W, Chen J W, He X, Sun S L, Yin Y L, Chen Z. Discrete element modeling and verification of the simulation parameters for chopped hybrid Broussonetia papyrifera stems. Int J Agric & Biol Eng, 2024; 17(1): 23–32.

[11] Hao J J, Wei W B, Huang P C, Qin J H, Zhao J G. Calibration and experimental verification of discrete element parameters of oil sunflower seeds. Transactions of the CSAE, 2021; 37(12): 36–44. (in Chinese)

[12] Hou Z F, Dai N Z, Chen Z, Chou Y, Zhang X W. Measurement and calibration of physical property parameters for Agropyron seeds in a discrete element simulation. Transactions of the CSAE, 2020; 36(24): 46–54. (in Chinese)

[13] Liu F Y, Zhang J, Chen J. Construction of visco-elasto-plasticity contact model of vibratory screening and its parameters calibration for wheat. Transactions of the CSAE, 2018; 34(15): 37–43. (in Chinese)

[14] Bai S H, Yuan Y W, Niu K, Zhou L M, Zhao B, Liu L J, et al. Simulation parameter calibration and experimental study of a discrete element model of cotton precision seed metering. Agriculture, 2022; 12(870): 1–20.

[15] Zhang G Z, Chen L M, Liu H P, Dong Z, Zhang Q H, Zhou Y. Calibration and experiments of the discrete element simulation parameters for water chestnut. Transactions of the CSAE, 2022; 38(11): 41–50. (in Chinese)

[16] Shu C X, Yang J, Wan X Y, Yuan J C, Liao Y T, Liao Q X. Calibration and experiment of the discrete element simulation parameters of rape threshing mixture in combine harvester. Transactions of the CSAE, 2022; 38(9): 34–43. (in Chinese)

[17] Ma Y H, Song C D, Xuan C Z, Wang H Y, Yang S, Wu P. Parameters

calibration of discrete element model for alfalfa straw compression simulation. Transactions of the CSAE, 2020; 36(11): 22–30. (in Chinese)

[18] Liu F Y, Zhang J, Chen J. Modeling of flexible wheat straw by discrete element method and its parameters calibration. Int J Agric & Biol Eng, 2018; 11(3): 42–46.

[19] Wu M C, Cong J L, Yan Q, Zhu T, Peng X Y, Wang Y S. Calibration and experiments for discrete element simulation parameters of peanut seed particles. Transactions of the CSAE, 2020; 36(23): 30–38. (in Chinese)

[20] Shi L R, Ma Z T, Zhao Wuyun, Yang X P, Sun B G, Zhang J P. Calibration of simulation parameters of flaxed seeds using discrete element method and verification of seed-metering test. Transactions of the CSAE, 2019; 35(20): 25–33. (in Chinese)

[21] Shi L R, Yang X P, Zhao W Y, Sun W, Wang G P, Sun B G. Investigation of interaction effect between static and rolling friction of corn kernels on repose formation by DEM. Int J Agric & Biol Eng, 2021; 14(5): 238–246.

[22] Fan G J, Wang S Y, Shi W J, Gong Z F, Gao M. Simulation parameter calibration and test of typical pear varieties based on discrete element method. Agronomy, 2022; 12(1720): 1–18.

[23] Song S L, Tang Z H, Zheng X, Liu J B, Meng X J, Liang Y C. Calibration of the discrete element parameters for the soil model of cotton field after plowing in Xinjiang of China. Transactions of the CSAE, 2021; 37(20): 63–70. (in Chinese)

[24] Xing J J, Zhang R, Wu Pg, Zhang X R, Dong X H, Chen Y, Ru S F. Parameter calibration of discrete element simulation model for latosol particles in hot areas of Hainan Province. Transactions of the CSAE, 2020; 36(5): 158–166. (in Chinese)

[25] Peng C W, Xu D J, He X, Tang Y H, Sun S L. Parameter calibration of discrete element simulation model for pig manure organic fertilizer treated with Hermetia illucen. Transactions of the CSAE, 2020; 36(17): 212–218. (in Chinese)

[26] Yuan Q C, Xu L M, Xing J J, Duan Z Z, Ma S, Yu C C, Chen C. Parameter calibration of discrete element model of organic fertilizer particles for mechanical fertilization. Transactions of the CSAE, 2018; 34(18): 21–27. (in Chinese)

[27] Xie F P, Wu Z Y, Wang X S, Liu D W, Wu B, Zhang Z Z. Calibration of discrete element parameters of soils based on unconfined compressive strength test. Transactions of the CSAE, 2020; 36(13): 39–47. (in Chinese)

[28] Yan D X, Yu J Q, Wang Y, Zhou L, Tian Y, Zhang. Soil particle modeling and parameter calibration based on discrete element method. Agriculture, 2022; 12(1421): 1–15.

[29] Ma S, Xu L M, Yuan Q C, Niu C, Zeng J, Chen C, Wang S S, Yuan X T. Calibration of discrete element simulation parameters of grapevine antifreezing soil and its interaction with soil-cleaning components. Transactions of the CSAE, 2020; 36(1): 40–49. (in Chinese)

[30] GB/T 1933-2009, Method for determination of the density of wood. Chian: General Administration of Quality Supervision, Inspection and Quarantine of the People's Republic of China, 2009. (in Chinese)

[31] GB/T 1931-2009, Method for determination of the moisture content of wood. Chian: General Administration of Quality Supervision, Inspection and Quarantine of the People's Republic of China, 2009. (in Chinese)

[32] Zhao F F. The tractive notoginseng harvester design and experimental research . Kunming: Kunming University of Science and Technology, 2016; 11–22. (in Chinese)

[33] Xie K T, Zhang Z G, Wang Y C, Tang J X, Yu X L. Simulation analysis and test of Panax notoginseng excavating shovel based on LS-DYNA. Journal of Northeast Agricultural University, 2021; 52(5): 79–88. (in Chinese)

[34] Zhang S W, Zhang R Y, Chen T Y, Fu J, Yuan H F. Calibration of simulation parameters of mung bean seeds using discrete element method and verification of seed-metering test. Transactions of the CSAM, 2022; 53(3): 71–79.

[35] JB/T 9014.7-1999, Determination of accumulated angle. China, Machinery Industry Standard, 2000. (in Chinese)

[36] Müller D, Fimbinger E, Brand C. Algorithm for the determination of the angle of repose in bulk material analysis. Powder Technology, 2021; 383: 598–605.

[37] Wang Y C. Study on mining mechanism of Panax notoginseng based on discrete element method . Kunming: Kunming University of Science and Technology, 2021; 11–33. (in Chinese)